2011

Evidence for two phases of galaxy formation from radial trends in the globular cluster system of NGC 1407

D. A. Forbes
L. R. Spitler
J. Strader
Aaron J. Romanowsky, *San Jose State University*
J. P. Brodie, et al.

Evidence for two phases of galaxy formation from radial trends in the globular cluster system of NGC 1407

Duncan A. Forbes,[1][*] Lee R. Spitler,[1] Jay Strader,[2] Aaron J. Romanowsky,[3]
Jean P. Brodie[3] and Caroline Foster[1]

[1]*Centre for Astrophysics & Supercomputing, Swinburne University, Hawthorn VIC 3122, Australia*
[2]*Harvard-Smithsonian Centre for Astrophysics, Cambridge, MA 02138, USA*
[3]*UCO/Lick Observatory, University of California Santa Cruz, CA 95064, USA*

ABSTRACT

Here we present the colours of individual globular clusters (GCs) around the massive elliptical galaxy NGC 1407 out to a projected galactocentric radius of 140 kpc or 17 galaxy effective radii (R_e). Such data are a proxy for the halo metallicity. We find steep, and similar, metallicity gradients of ~ -0.4 dex dex^{-1} for both the blue (metal poor) and red (metal rich) GC subpopulations within 5–8.5 R_e (40–70 kpc). At larger radii the mean GC colours (metallicity) are constant. A similar behaviour is seen in a wide-field study of M87's GC system, and in our own Galaxy. We interpret these radial metallicity trends to indicate an inner region formed by early *in situ* dissipative processes and an outer halo formed by the ongoing accretion of low-mass galaxies and their GCs. These results provide observational support for the model of galaxy formation whereby massive galaxies form inside-out in two phases. We have also searched the literature for other massive early-type galaxies with reported GC metallicity gradients in their inner regions. No obvious correlation with galaxy mass or environment is found but the sample is currently small.

Key words: globular clusters: general – galaxies: formation – galaxies: individual: NGC 1407 – galaxies: star clusters: general.

1 INTRODUCTION

An emerging picture of galaxy formation is that massive early-type galaxies grow from relatively compact 'seed' galaxies with effective radii of $\sim$1 kpc at $z \geq 2$ (sometimes referred to as 'red nuggets') to today's massive systems of effective radii of $\sim$5 kpc (Gobat et al. 2011; Oser et al. 2010). This size evolution has a redshift dependence of the form $(1 + z)^{-1.2}$ (Franx et al. 2008; Williams et al. 2010) and is driven by the growth of the outer regions of galaxies that experience ongoing accretion (van Dokkum et al. 2010).

According to theory, the growth of stellar mass occurs in two phases: (1) An *in situ* dissipative phase with cold flows (Kereš et al. 2005; Dekel, Sari & Ceverino 2009; Naab, Johansson & Ostriker 2009; Oser et al. 2010) that is reminiscent of a 'monolithic collapse' (Larsen 1975) and (2) ongoing accretion from minor mergers of lower mass systems (Abadi, Navarro & Steinmetz 2006; Hopkins et al. 2009; Zolotov et al. 2010). The *in situ* stars form, and are in place, early in the Universe (i.e. $\geq$10 Gyr ago), whereas the outer halo experiences a more continuous growth as additional material

is accreted over time. The transition between the *in situ* dominated inner regions and the accretion-dominated outer halo is predicted to occur at radii of tens of kiloparsecs (Abadi et al. 2006; Zolotov et al. 2010), with more massive galaxies undergoing more accretion and having larger transition radii (Oser et al. 2010).

This theoretical picture is difficult to test observationally. For very nearby ($\sim$10 Mpc) early-type galaxies, individual stars can be resolved by the *Hubble Space Telescope* (*HST*) and the radial metallicity distribution probed. For example, in NGC 3379 the halo shows a metallicity transition at 10–13 R_e, becoming metal poor (Harris et al. 2007). Only a handful of massive galaxies can be studied in this way.

Integrated light observations are required to obtain the metallicity distribution for more distant galaxies. However, the surface brightness profiles of early-type galaxies fall off rapidly with galactocentric radius making it difficult to probe beyond a few effective radii. An example is the recent work of Coccato, Gerhard & Arnaboldi (2010) who, after 13.5 h of integration on an 8-m telescope, obtained stellar population gradients in the massive Coma elliptical galaxy NGC 4889 to an unprecedented 4 R_e. They derived metallicity, alpha element and age gradients from an analysis of the absorption lines using Lick indices. They found a 'break' radius at $\sim$1.2 R_e (18 kpc) dividing the inner galaxy that exhibited a

steep metallicity gradient and high alpha element ratio (indicative of rapid star formation) from the outer region that had a metallicity gradient consistent with zero and evidence for more prolonged star formation. They described the inner region as formed in an early dissipative collapse and the outer region as having an accreted origin. Given the telescope time involved it will be difficult to repeat such a study for a large sample of ellipticals.

Another tracer of halo stellar populations is therefore required. Globular clusters (GCs) have many advantages in this regard. As some GCs are destroyed over time, they contribute directly to the halo field star population. In the case of the Milky Way, about 1/3 of the original GC system may have been destroyed (Mackey & van den Bergh 2005) making up half of the current halo stellar mass (Martell & Grebel 2010). When a low-mass galaxy is accreted by a larger one, GCs can survive the accretion process (Forbes & Bridges 2010) and the properties of these GCs contain information about their original host galaxy. Also, GC systems can extend beyond 100 kpc and hence they probe galaxy haloes to many effective radii.

The globular cluster systems of large galaxies are generally found to consist of two subpopulations – blue (or metal poor) and red (or metal rich). These are thought to be associated with the halo and bulge/spheroid component of galaxies, respectively (Brodie & Strader 2006). The mean colour of both subpopulations have been shown to correlate with the luminosity or mass of the host galaxy, with some possible flattening of the relation for low-mass galaxies (Forbes, Brodie & Grillmair 1997; Larsen et al. 2001; Strader, Brodie & Forbes 2004; Peng et al. 2006). We note that the mean colour used in such studies is generally derived from the central regions of a galaxy. Recent studies of extragalactic GC systems have revealed two additional trends: the colour (metallicity) of GCs with their magnitude (mass) and colour with projected galactocentric radius.

The first trend, called the 'blue tilt' (a tendency for the blue GCs to have redder colours at brighter magnitudes), was first discovered using the Advanced Camera for Surveys (ACS) on the *HST* to examine extragalactic GC systems. The ACS provides highly accurate photometry and GC candidate lists that are largely free of contaminants (due to the fact that GCs are partially resolved out to distances of ∼20 Mpc). The blue tilt has now been reported in a variety of galaxies including the most massive ellipticals (Harris et al. 2006; Harris 2009a), lower mass ellipticals (Strader et al. 2006), early-type dwarfs (Mieske et al. 2006a), early-type spirals (Spitler et al. 2006) and a Milky Way like spiral (Forbes et al. 2010). It has not been detected in the Milky Way GC system (most likely due to the small number of massive GCs) nor the massive elliptical NGC 4472 (Mieske et al. 2006a; Strader et al. 2006) despite its large GC system.

Given the evidence that extragalactic GCs are mostly old (Brodie & Strader 2006), the blue tilt implies a mass–metallicity relation for the metal-poor subpopulation of GCs. Various explanations have been proposed (see Mieske et al. 2006a; Bekki et al. 2007; Mieske 2009), but perhaps the most plausible explanation to date is one of self-enrichment, whereby more massive GCs are enriched with heavier metals during their brief formation period (Parmentier 2004; Strader & Smith 2008; Bailin & Harris 2009).

The second trend, whereby the mean colour of each GC subpopulation varies with galactocentric radius, was first seen in ground-based photometry of M49 using metallicity-sensitive filters (Geisler, Lee & Kim 1996). Such a trend needs to be carefully separated from the trend of a declining mean colour with radius in the *overall* GC system (due to the changing relative proportions of blue and red subpopulations), and has only been measured for a handful of other

systems (Forte et al. 2001; Bassino et al. 2006; Harris 2009a,b). These studies indicate a negative metallicity gradient for both the blue and red subpopulations in elliptical galaxies. In the case of the Milky Way, a metallicity gradient is seen in both GC subpopulations within the central 10 kpc of slope ≈ −0.30 dex dex^{-1} (Harris 2001). Beyond 10 kpc, the mean GC metallicity in the Galactic halo is constant at [Fe/H] ∼ −1.5. The M31 GC system reveals a strong metallicity gradient within 50 kpc, but flattens out to a near-constant metallicity of [Fe/H] ∼ −1.6 (Alves-Brito et al. 2009). These strong metallicity gradients in the inner halo regions suggest a dissipative formation process *for both GC subpopulations*.

Here we present the radial distribution of GC colour (and hence metallicity) using deep wide-field Subaru imaging of the massive elliptical galaxy NGC 1407 out to ∼140 kpc or 17 R_e. We find a strong radial gradient which is supported by *HST* imaging and Keck spectroscopy. We compare the radial gradient to those of other massive ellipticals, finding that the gradient in the NGC 1407 GC system is the steepest published to date. We briefly discuss the wider implications for galaxy formation from our results.

2 NGC 1407

NGC 1407 is the central massive elliptical in a large group (Brough et al. 2006) with a rich globular cluster system (Forbes et al. 2006). The galaxy itself reveals a steep metallicity gradient in the starlight (Spolaor et al. 2008; Foster et al. 2009) and is uniformly old with a supersolar alpha element ratio within 1 effective radius. Our previous optical spectra of 20 bright GCs in NGC 1407 indicated that they are mostly old (∼11 Gyr) with a range of metallicity −1.5 < [Z/H] < 0.0 (Cenarro et al. 2007). Some of the spectra showed evidence for the presence of blue horizontal branch stars. Our previous dynamical study of the GC system (Romanowsky et al. 2009) found weak evidence for rotation and a bias towards tangential orbits in the outer regions. We derived a total virial halo mass of 6×10^{13} M$_\odot$ which indicates that NGC 1407 and its surrounding group is extremely dark (with $M/L_B \sim 800$). We assume an effective radius for NGC 1407 itself of 1.17 arcmin as adopted by Harris (2009a) and Foster et al. (2009).

Images of NGC 1407 have been taken using the ACS camera on board the *HST* using F435W (B) and F814W (I) filters covering 3.5×3.5 arcmin^2. An analysis of the GC system using these data has been reported by Forbes et al. (2006), Harris et al. (2006) and Harris (2009a). The GC system reveals a classic blue/red bimodality with a blue tilt in the blue subpopulation.

Harris (2009a) studied the colour–radius distribution for the NGC 1407 GC system finding an insignificant (1σ) trend for both the blue and red GCs examined. However, when the NGC 1407 GC system was combined with that of five other massive elliptical galaxies, a statistically significant metallicity gradient of −0.10 dex dex^{-1} was seen at >4.5σ for both subpopulations.

The distance to NGC 1407 is somewhat uncertain. Here we adopt the mean value of 15 distances given by NED i.e. $m - M = 31.85 \pm 0.37$ (or 23.77 ± 3.8 Mpc). At this distance, 1 arcmin equals 6.9 kpc.

3 PHOTOMETRIC DATA

Here we use wide-field (34×27 arcmin^2) g, r and i images taken using the Suprime-Cam camera on the Subaru 8-m telescope. Total exposure times were 3, 1 and 0.9 h for the g, r and i images, respectively. The seeing was good at around 0.5 arcsec in each filter. The Suprime-Cam has a pixel scale of 0.2 arcsec pixel^{-1}. Full details

of the observations, data reduction and analysis will be presented in Spitler et al. (in preparation). Here we give a brief summary.

The images were reduced and combined using the Suprime-Cam standard pipeline software. The final mosaic was placed on the USNO-B2 astrometric system using common stars. Before the initial object detection, a smooth model of NGC 1407 (and the galaxy NGC 1400, which lies at a projected separation of 12 arcmin) was subtracted, using the ELLIPSE task in IRAF to help with object detection. DAOFIND was then used to select objects with a threshold ~3 times the standard deviation of the background count level.

For each point-like object an aperture magnitude and position was measured. Aperture magnitudes were corrected to total magnitudes assuming that the objects were point sources (a reasonable assumption for GCs with an average expected size of 3 pc or 0.03 arcsec under 0.5-arcsec seeing) and applying filter-dependent aperture corrections. These were converted to standard magnitudes using zero-points determined with standard star observations. Extinction corrections using the maps of Schlegel, Finkbeiner & Davis (1998) were applied assuming no variation across the image as NGC 1407 is known to be relatively free of dust from mid-IR observations (Temi, Brighenti & Mathews 2009). Hereafter we quote extinction-corrected magnitudes and colours. A colour selection was applied so that objects within 1σ of the GC sequence in $g - r$ and $r - i$ colour–colour parameter space (i.e. $0.4 < g - i < 1.4$ and $0.3 < g - r < 0.9$) were included.

Finally, any GC candidates associated within 6-arcmin radius of NGC 1400 were removed from the object list for the subsequent analysis. This effectively removes any possible contamination from the GC system of NGC 1400.

4 RESULTS

In Fig. 1 we show the distribution of GC colour with projected galactocentric radius out to 20 arcmin from our wide-field Subaru imaging. As well as the individual data points we show the mean
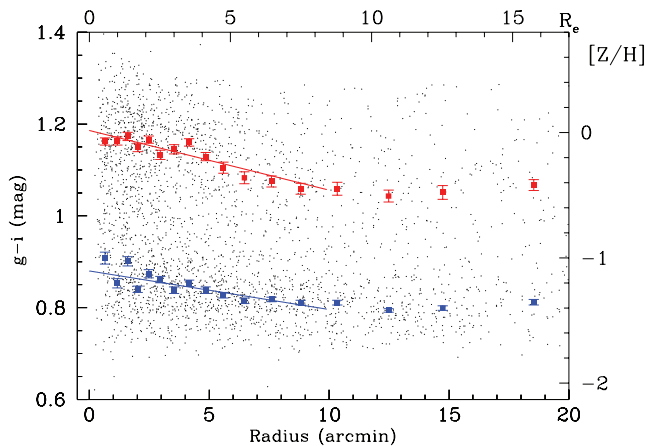
Figure 1. Globular cluster colour–radial distribution from Subaru photometry. The small circles show individual GCs from Subaru photometry with $i < 24$ (and errors $\leq$0.03 mag). Mean colours and error on the mean are represented by filled squares. The solid lines show the best-fitting linear gradient within 10 arcmin. The top and right axes show transformations into effective radius and metallicity, respectively. Both subpopulations show a strong gradient in mean colour within the central ~10 arcmin (8.5 R_e, 69 kpc). The galaxy starlight at 1 R_e has a colour $g - i \sim 1.2$, similar to the mean colour of the red GCs.

value and error on the mean in several radial bins using the NMIX statistical test (Richardson & Green 1997). The figure shows only those GCs with $i < 24$ ($M_i > -7.9$). The data show evidence for a clear negative metallicity gradient out to ~6–10 arcmin (5–8.5R_e or 40–70 kpc) and are consistent with zero gradient beyond that. A simple linear fit to radii within 10 arcmin gives central colours of $g - i = 0.880 \pm 0.011$ and 1.186 ± 0.007 for the blue and red subpopulations, respectively. Similarly, the slopes are found to be -0.0084 ± 0.022 and -0.013 ± 0.002 mag arcmin^{-1}. Thus the blue subpopulation gradient is at the ~4σ level and the red one at the ~6σ.

Following the method of Harris (2009b) we also fit the entire colour gradient with the form $g - i = a + b \log (R/R_e)$, where $R_e = 1.17$ arcmin. We fit only the data points interior to ~10 arcmin (although including radial bins beyond this radius makes little difference to the final values). For the blue subpopulation we find $a = 0.818 \pm 0.01$ and $b = -0.063 \pm 0.01$ mag dex^{-1}. Similarly for the red subpopulation we find $a = 1.12 \pm 0.02$ and $b = -0.068 \pm 0.02$ mag dex^{-1}. For both subpopulations the uncertainty quoted comes from the range of fits that include/exclude the innermost data point (the steeper slope being associated with an exclusion of the innermost radial bin). Within the combined errors, the blue and red GC subpopulations show a similar colour gradient.

To convert the $g - i$ colour gradients into metallicity gradients we follow Harris (2009a) i.e. $\Delta g - i = 0.21\Delta$[Fe/H], giving metallicity gradients of -0.38 ± 0.06 dex dex^{-1} for the blues and -0.43 ± 0.07 dex dex^{-1} for the reds.

We also show in Fig. 1 metallicities corresponding to $g - i$ colours assuming the linear relation found by Sinnott et al. (2010). This relation is in part based on Milky Way GC metallicities from Harris (1996) which is close to the Carretta & Gratton (1997) scale and hence we assume is closer to total metallicity [Z/H] (see also discussion by Mendel, Proctor & Forbes 2007).

We have calculated the probability density function (PDF) for the data shown in Fig. 1 in six radial bins (centred on 0.92, 1.81, 2.72, 3.85, 5.23 and 7.04 arcmin) of equal GC number. The PDF is sensitive to colour substructure and is shown graphically in Fig. 2. Other than the innermost radial bin, the PDF for the blue GCs confirms their radial colour gradient. For the red GCs the radial trend is less clear due to possible colour substructure in the inner regions.

In Fig. 3 we show the distribution of GC colour with galactocentric radius from the *HST* ACS imaging (Forbes et al. 2006). These data have the advantage of having a lower contamination rate than the Subaru imaging (which we estimate to be less than 5 per cent for bright GCs based on follow-up spectra; Romanowsky et al. 2009) but probe to much smaller galactocentric radii. Again we show the mean colours and the error on the mean in various radial bins with equal numbers of GCs. A clear colour gradient is seen in the red subpopulation and to a lesser extent in the blue subpopulation supporting our Subaru results above. Fitting $B - I = a + b \log (R/R_e)$ we find $a = 1.62 \pm 0.02$ and $b = -0.147 \pm 0.065$ dex dex^{-1} for the blue subpopulation and $a = 2.05 \pm 0.01$ and $b = -0.169 \pm 0.005$ dex dex^{-1} for the red GCs.

Assuming a conversion of $B - I$ colour into metallicity of $\Delta B - I = 0.375\Delta$[Fe/H] (Harris 2009b), these slopes give a metallicity gradient of -0.39 ± 0.17 dex dex^{-1} for the blues and -0.45 ± 0.01 dex dex^{-1} for the reds. These values are identical to those inferred from the larger radii $g - i$ gradient.

We also show in Fig. 3 the metallicities corresponding to $B - I$ colours assuming the linear relation quoted by Harris (2009b). As for the $g - i$ colours, this relation based on Milky Way GC
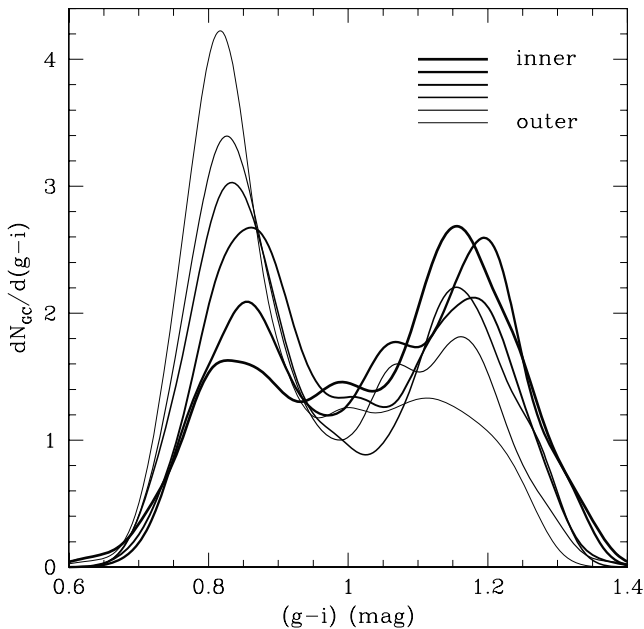
Figure 2. Globular cluster colour–radius probability density function (PDF). The curves show the PDF in six radial bins from inner (thick line) to outer (thin line). Other than the innermost radial bin the blue GCs show a steady trend of getting bluer with radius. For the red GCs the radial trend is less clear due to possible colour substructure in the inner regions.
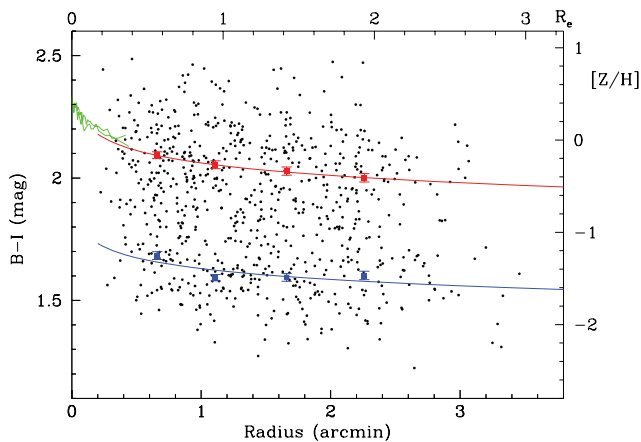
Figure 3. Globular cluster colour–radial distribution from *HST* photometry. The small circles show individual GCs from *HST* photometry. Mean colours and error on the mean are represented by filled squares. The top and right axes show transformations into effective radius and metallicity, respectively. The solid lines show the best-fitting gradient in colour–log radius space. The galaxy starlight at $1\,R_e$ has a colour $B-I \sim 2.2$, similar to the mean colour of the red GCs. The green lines within $0.5R_e$ show the galaxy field star metallicity from Spolaor et al. (2008).

metallicities from Harris (1996) which is close to the Carretta & Gratton (1997) scale and hence total metallicity [Z/H].

The radial stellar population properties for the NGC 1407 field stars out to $\sim 0.5R_e$ have been measured, from an analysis of the absorption lines, by Spolaor et al. (2008). They found the galaxy to have a central total metallicity of $[Z/H] \sim +0.3$ dex and a steep metallicity gradient of -0.38 ± 0.04 dex dex^{-1}. These values are similar to those found for the red GCs in NGC 1407 and are illustrated in Fig. 3. The error on individual points from Spolaor et al. is ± 0.15 dex. This supports previous claims that the red GCs are

closely associated with the bulge/spheroid component of elliptical galaxies (Forbes & Forte 2001; Forte, Vega & Favio 2009; Spitler 2010). The metallicity gradient of Foster et al. (2009) has a similar slope but has individual errors of ± 1 dex (and is not shown).

Could the colour gradient for the blue subpopulation seen in Figs 1–3 simply be due to a changing strength of the blue tilt with radius? For this to be the case the blue tilt would need to be significantly stronger (i.e. tilted more to the red at bright magnitudes) in the inner galaxy regions and to disappear (i.e. no blue tilt) for galactocentric radii beyond ~ 10 arcmin. Mieske et al. (2006a, 2010) found weak evidence for a stronger blue tilt at small galactocentric radii in their data for Virgo and Fornax early-type galaxies. However, for the large galaxies in their study, they were generally restricted to the inner $\sim 1.5R_e$ due to the *HST* ACS field-of-view. Harris (2009a) explored this issue out to $\sim 5R_e$ using a composite of the GC systems in six giant ellipticals, finding no convincing evidence for a stronger blue tilt in the inner regions. Further evidence comes from the fact that NGC 4472 reveals a radial gradient (Geisler et al. 1996) but no blue tilt (Strader et al. 2006).

We have divided the Subaru data into three radial bins i.e. to a projected galactocentric radius of 5 arcmin, between 5 and 10 arcmin and beyond 10 arcmin. All three radial bins reveal a blue tilt of similar strength. The relatively constant strength of the blue tilt with radius cannot explain the observed gradient in the mean colour with radius within 10 arcmin (nor the lack of a gradient beyond 10 arcmin). We thus conclude that the colour gradient observed in the blue subpopulation is not caused by a changing colour–magnitude trend with radius. Finally, the radial metallicity gradient of the blue subpopulation is similar to that of the red GCs, which do not show a 'red tilt'.

Could the GC colour gradients be due to contamination? The radial surface density profiles of the blue and red GC candidates around NGC 1407 (Spitler et al., in preparation), show that they are dominated by objects that are associated with NGC 1407 for radii <10 arcmin (i.e. for which the strong metallicity gradient is seen). Based on these profiles the estimated contamination rate at 10 arcmin is less than 20 per cent for the blue GCs but could be as high as 50 per cent for the red GCs. Thus the transition radius for the blue GCs appears to be robust but the flattening of the gradient for the red GCs at large radii could be an artefact of increased contamination.

Foster et al. (2010) explored the use of the Calcium Triplet (CaT) lines to derive spectroscopic metallicities for GCs in NGC 1407 but did not explore the radial variation of CaT metallicity for the GC subpopulations. Using a linear CaT to metallicity transformation based on Milky Way GCs by Armandroff & Zinn (1988), they found the red GCs to have reasonable metallicities but the blue GCs had inferred metallicities that were too high i.e. they had stronger CaT strengths than expected. This could be due to an extra contribution from blue horizontal branch stars (as suggested by Cenarro et al. 2007 for the NGC 1407 GCs). In Fig. 4 we plot the CaT-derived metallicities (converted to total metallicity assuming $[Z/H] = [Fe/H] + [\alpha/Fe]$, where $[\alpha/Fe]$ is assumed to have a constant value of 0.3 typical of Milky Way GCs). The data, taken with the DEIMOS spectrograph on the Keck telescope, have been restricted to GCs with S/N ≥ 12. We show the red and blue GCs separately. The blue GCs show significant scatter about a mean value of $[Z/H] \sim -0.5$, again suggesting a problem with their derived metallicities [see Foster et al. (2010) for a full discussion for this and possible explanations]. The red GCs, on the other hand, show a clear radial gradient. Here we overplot the total metallicity gradient derived from Fig. 1 on the red GCs. Although not a fit to the data, the
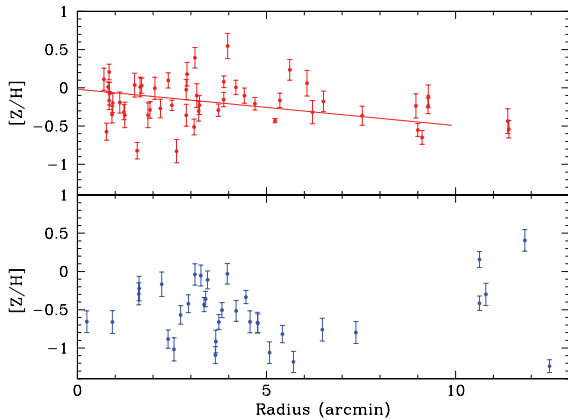
Figure 4. Globular cluster metallicity–radial distribution derived from calcium triplet measurements. The top panel shows the red GC subpopulation, and the bottom panel shows the blue GC subpopulation. A clear radial gradient is seen in the red GC subpopulation. The solid line shown in the top panel is not a fit to the data but rather the metallicity gradient from Fig. 1 superposed.

metallicity gradient based on $g - i$ colour provides a remarkably good representation of the overall red GC trend.

5 DISCUSSION

From deep wide-field imaging we find a transition from a strong colour gradient in both GC subpopulations which flattens to a constant value, with the transition occurring at a projected radius of around 6–10 arcmin. Approximately half of the GCs are located within this radius. At a slightly larger radius ($\sim$12 arcmin) Zhang et al. (2007) report that the X-ray surface brightness around NGC 1407 declines to a near-constant value, which they refer to as the 'gas halo boundary'.

The behaviour of the NGC 1407 GC colour profiles are similar to those in the Milky Way, for which strong gradients (-0.30 dex dex^{-1}; Harris 2001) are seen in both the red and blue GCs interior to 10 kpc and a constant metallicity of [Fe/H] ~ -1.5 for the blue GCs at larger radii (there are essentially no red GCs beyond 10 kpc). The gradient seen in the NGC 1407 GC system is the strongest reported to date in an elliptical galaxy, with the previous strongest gradient being -0.28 dex dex^{-1} in the NGC 1399 GC system reported by Bassino et al. (2006). We note that the actual 3D gradients may be stronger than those observed in projection.

Most previous detections of GC subpopulation colour gradients in early-type galaxies have been generally restricted to $\leq 5R_e$ and may not extend far enough to probe the accretion-dominated region of the haloes of massive galaxies. One exception is the wide-field study of M87 by Harris (2009a) using CFHT Megacam which allowed the GC system to be probed to $\sim 20R_e$. To quote Harris *This [metallicity gradient] feature is clearest for $R \leq 8\,R_e$ or about 60 kpc; beyond that point, the red clusters are almost absent and the blue clusters show no significant change in mean colour.* Thus the GC system of M87 also appears to reveal a transition, at a similar scale in both effective radius and kpc to the NGC 1407 GC system.

The transition from a strong GC metallicity gradient to a constant value may represent a transition from a dissipative process (e.g. a gaseous collapse or gas-fed flows) to a dissipationless one (e.g. accretion of low-mass galaxies). This is in qualitative agreement with the recent simulations of galaxy formation in two phases (e.g. Naab

et al. 2009; Oser et al. 2010). In this model, the first *in situ* phase is associated with a dissipative collapse, which is followed by an extended phase of ongoing accretion of low-mass galaxies. More massive galaxies have larger transition radii. In this picture galaxies are built from inside-out. In the dissipational merger simulations of Hopkins et al. (2009) the outer constant metallicity is determined by the metallicity of the progenitor galaxies.

An alternative explanation is that the observed colour profile is caused by a changing relative mix of inner GCs that have fixed colours, and outer GCs that are bluer on average. Thus as the fraction of outer bluer GCs increases with radius a mean colour gradient is observed until the transition radius is reached, when the outer GCs completely dominate the overall GC colours (beyond 70 kpc in the case of NGC 1407). Such a situation could in principle be set up by a series of dry mergers without invoking dissipation; however, it would need to be fine-tuned in the sense of giving similar observed metallicity gradients for both the blue and red subpopulations and to occur at similar transition radii.

A kinematic analysis of 172 GCs around NGC 1407 revealed a bias towards tangential orbits with increasing galactocentric radius (Romanowsky et al. 2009). This orbital anisotropy is difficult to reconcile with either mergers or an accretion origin for the GCs. However, the study was largely confined to radii within 8 arcmin.

We note that kinematic transitions at large radii have now been reported in a handful of massive early-type galaxies based on the analysis of their stellar light and planetary nebulae as well as their GC systems (Coccato et al. 2009; Proctor et al. 2009; Arnold et al. 2011; Foster et al. 2010). However, more work is needed to increase radial sampling and the number of galaxies studied.

Prompted by trends between the metallicity gradient of the galaxy starlight and galaxy mass from both observations (e.g. Spolaor et al. 2009) and theory (e.g. Tortora et al. 2011), we have collated the statistically significant (i.e. more than 2σ) GC metallicity gradients from the literature and central velocity dispersions (a proxy for galaxy mass). Table 1 shows that there is no obvious trend between the GC metallicity gradient and the mass of the host galaxy (as traced by the central velocity dispersion); however, the sample is small and covers a limited range in host galaxy mass and environment.

The presence of two GC subpopulations in most galaxies is strong evidence that galaxies did not form by a *simple* monolithic collapse. The two phases of formation for NGC 1407 described here, support this view. Indeed, the *in situ* GCs appear to have formed in an early dissipative event as envisaged by Forbes et al. (1997). Here we have shown that *both* GC subpopulations appear to have taken part giving rise to similar strength metallicity gradients and transition radii. The accreted GCs provide an important contribution as envisaged in the scenario of Cote, Marzke & West (1998). However, in their scenario for the GC systems of massive galaxies, only the red GCs were involved in a dissipative formation event and the blue GCs were all accreted.

6 CONCLUSIONS

Using deep wide-field imaging from the Subaru Suprime-Cam we have explored the variation of GC colour (and hence metallicity) with galactocentric radius. We detect GCs out to $\sim$20 arcmin or 17 galaxy effective radii (R_e). This corresponds to $\sim$140 kpc for an assumed distance of 23.77 Mpc. This is therefore one of the most extended radial studies of a GC system to date.

We find that both the blue and red GC subpopulations reveal a strong colour gradient within $\sim$6–10 arcmin (40–70 kpc) or

Table 1. Globular cluster system metallicity–radius gradients in units of dex dex^{-1}. The central velocity dispersion (in km s^{-1}) comes from the Hyperleda data base. The source of each globular metallicity gradient is given in the last column. The metallicity gradients are converted from colour gradients assuming an old stellar population. The 1σ uncertainty when available is given in brackets.

Galaxy	Environ.	σ_0	Blue	Red	Source
NGC 1407	Group	272	−0.38 (0.06)	−0.43 (0.07)	This work
NGC 4472	Cluster	294	−0.15 (0.03)	−0.12 (0.06)	Geisler et al. (1996)
NGC 1399	Cluster	342	−0.2	−0.2	Forte et al. (2001)
NGC 1399	Cluster	342	−0.28 (0.06)	–	Bassino et al. (2006)
M87	Cluster	334	−0.12 (0.03)	−0.17 (0.03)	Harris (2009a)
NGC 3268	Group	224	−0.11 (0.05)	–	Harris (2009b)
NGC 4696	Cluster	254	−0.10 (0.04)	–	Harris (2009b)
NGC 7626	Group	271	−0.16 (0.06)	−0.18 (0.07)	Harris (2009b)
6 gEs	Cluster/Group	–	−0.10 (0.02)	−0.10 (0.02)	Harris (2009b)

5–8.5 R_e. Beyond this, the mean GC colours are constant. The presence of a colour gradient within the inner 3 arcmin is supported by *HST* ACS imaging. When converted into metallicity, the gradient for the red GC subpopulation is similar to that for the field stars in the central ~0.5R_e. We also report a spectroscopic metallicity gradient in the inner 10 arcmin based on CaT measurements from the Keck DEIMOS spectrograph.

The change from a strong GC metallicity gradient to a constant metallicity may indicate the transition between an inner halo formed by *in situ* dissipative processes, with both GC subpopulations taking part, to an outer one that is largely due to accretion of minor mergers. This transition radius is similar to the hot gas boundary seen in X-ray brightness profile of NGC 1407.

We find that the colour gradient seen in the blue GC subpopulation is not due to a changing 'blue tilt' strength with radius. Therefore, if the blue tilt is due to a self-enrichment process it does not appear to have a strong radial, or environmental, dependence.

We have searched the literature for statistically significant GC metallicity gradients in elliptical galaxies. We do not find a trend with host galaxy mass; however, the sample is small and largely restricted to massive galaxies in clusters/groups. We note that previous work on the correlation between mean GC colour and host galaxy mass has generally been restricted to galaxy central regions. Future wide-field studies of GC system radial colour gradients in a wider range of host galaxies and environments may reveal new trends and hence further insight into the galaxy formation process. Such a study is relatively inexpensive in terms of telescope time.

Our results provide observational support for the mass growth of massive elliptical galaxies in two phases i.e. early dissipative collapse followed by ongoing accretion of low-mass systems (e.g. Oser et al. 2010). In other words, elliptical galaxies form inside-out.

REFERENCES

Abadi M. G., Navarro J. F., Steinmetz M., 2006, MNRAS, 365, 747
Alves-Brito A., Forbes D., Mendel J., Hau G., Murphy M., 2009, MNRAS, 395, L34
Armandroff T. E., Zinn R., 1988, AJ, 96, 92
Arnold J., Romanowsky A., Chomiuk L., Spitler L., Strader J., Benson A., Forbes D., 2011, ApJ, submitted
Bailin J., Harris W. E., 2009, ApJ, 695, 1082
Bassino L. P., Faifer F. R., Forte J. C., Dirsch B., Richtler T., Geisler D., Schuberth Y., 2006, A&A, 451, 789
Bekki K., Yahagi H., Nagashima M., Forbes D. A., 2007, MNRAS, 382, L87
Brodie J. P., Strader J., 2006, ARA&A, 44, 193
Brough S., Forbes D. A., Kilborn V. A., Couch W., Colless M., 2006, MNRAS, 369, 1351
Carretta E., Gratton R. G., 1997, A&AS, 121, 95
Cenarro A. J., Beasley M. A., Strader J., Brodie J. P., Forbes D. A., 2007, AJ, 134, 391
Coccato L. et al., 2009, MNRAS, 394, 1249
Coccato L., Gerhard O., Arnaboldi M., 2010, MNRAS, 407, L26
Cote P., Marzke R. O., West M. J., 1998, ApJ, 501, 554
Dekel A., Sari R., Ceverino D., 2009, ApJ, 703, 785
Forbes D. A., Bridges T., 2010, MNRAS, 404, 1203
Forbes D. A., Forte J.-C., 2001, MNRAS, 322, 257
Forbes D. A., Brodie J. P., Grillmair C. J., 1997, AJ, 113, 1652
Forbes D. A., Sánchez-Blázquez P., Phan A. T. T., Brodie J. P., Strader J., Spitler L., 2006, MNRAS, 366, 1230
Forbes D. A., Spitler L. R., Harris W. E., Bailin J., Strader J., Brodie J. P., Larsen S. S., 2010, MNRAS, 403, 429
Forte J. C., Geisler D., Ostrov P. G., Piatti A. E., Gieren W., 2001, AJ, 121, 1992
Forte J. C., Vega E., Favio F., 2009, MNRAS, 397, 1003
Foster C., Proctor R. N., Forbes D. A., Spolaor M., Hopkins P. F., Brodie J. P., 2009, MNRAS, 400, 2135
Foster C., Forbes D. A., Proctor R. N., Strader J., Brodie J. P., Spitler L. R., 2010, AJ, 139, 1566
Franx M., van Dokkum P. G., Schreiber N. M. F., Wuyts S., Labbé I., Toft S., 2008, ApJ, 688, 770
Geisler D., Lee M. G., Kim E., 1996, AJ, 111, 1529
Gobat R. et al., 2011, A&A, 526, A133
Harris W. E., 1996, AJ, 112, 1487
Harris W. E., 2001, in Star Clusters, Saas Fee Advanced Course 28. Springer, Berlin
Harris W. E., 2009a, ApJ, 699, 254
Harris W. E., 2009b, ApJ, 703, 939

Harris W. E., Whitmore B. C., Karakla D., Okoń W., Baum W. A., Hanes D. A., Kavelaars J. J., 2006, ApJ, 636, 90

Harris W. E., Harris G. L. H., Layden A. C., Wehner E. M. H., 2007, ApJ, 666, 903

Hopkins P. F., Cox T. J., Dutta S. N., Hernquist L., Kormendy J., Lauer T. R., 2009, ApJS, 181, 135

Kereš D., Katz N., Weinberg D. H., Davé R., 2005, MNRAS, 363, 2

Larsen E. W., 1975, J. Quant. Spectrosc. Radiative Transfer, 15, 1

Larsen S. S., Brodie J. P., Huchra J. P., Forbes D. A., Grillmair C. J., 2001, AJ, 121, 2974

Mackey A. D., van den Bergh S., 2005, MNRAS, 360, 631

Martell S. L., Grebel E. K., 2010, A&A, 519, A14

Mendel J., Proctor R., Forbes D., 2007, MNRAS, 379, 1618

Mieske S., 2009, in Richtler T., Larsen S., eds, ESO Astrophysics Symposia, Globular Clusters: Guides to Galaxies. Springer, Berlin

Mieske S. et al., 2006a, ApJ, 653, 193

Mieske S., Hilker M., Infante L., Jordan A., 2006b, AJ, 131, 2442

Mieske S. et al., 2010, ApJ, 710, 1672

Naab T., Johansson P. H., Ostriker J. P., 2009, ApJ, 699, L178

Oser L., Ostriker J. P., Naab T., Johansson P. H., Burkert A., 2010, ApJ, 725, 2312

Parmentier G., 2004, MNRAS, 351, 585

Peng E. W. et al., 2006, ApJ, 639, 95

Proctor R. N., Forbes D. A., Romanowsky A. J., Brodie J. P., Strader J., Spolaor M., Mendel J. T., Spitler L., 2009, MNRAS, 398, 91

Richardson S., Green P., 1997, J. R. Statistical Soc. B, 59, 731

Romanowsky A. J., Strader J., Spitler L. R., Johnson R., Brodie J. P., Forbes D. A., Ponman T., 2009, AJ, 137, 4956

Schlegel D. J., Finkbeiner D. P., Davis M., 1998, ApJ, 500, 525

Sinnott B., Hou A., Anderson R., Harris W. E., Woodley K. A., 2010, AJ, 140, 2101

Spitler L. R., 2010, MNRAS, 406, 1125

Spitler L. R., Larsen S. S., Strader J., Brodie J. P., Forbes D. A., Beasley M. A., 2006, AJ, 132, 1593

Spolaor M., Forbes D. A., Proctor R. N., Hau G. K. T., Brough S., 2008, MNRAS, 385, 675

Spolaor M., Proctor R., Forbes D., Couch W., 2009, ApJ, 691, 138

Strader J., Smith G. H., 2008, AJ, 136, 1828

Strader J., Brodie J. P., Forbes D. A., 2004, AJ, 127, 3431

Strader J., Brodie J. P., Spitler L., Beasley M. A., 2006, AJ, 132, 2333

Temi P., Brighenti F., Mathews W. G., 2009, ApJ, 707, 890

Tortora C., Romeo A. D., Napolitano N. R., Antonuccio-Delogu V., Meza A., Sommer-Larsen J., Capaccioli M., 2011, MNRAS, 411, 627

van Dokkum P. G. et al., 2010, ApJ, 709, 1018

Williams R. J., Quadri R. F., Franx M., van Dokkum P., Toft S., Kriek M., Labbé I., 2010, ApJ, 713, 738

Zhang Z., Xu H., Wang Y., An T., Xu Y., Wu X.-P., 2007, ApJ, 656, 805

Zolotov A., Willman B., Brooks A. M., Governato F., Hogg D. W., Shen S., Wadsley J., 2010, ApJ, 721, 738

This paper has been typeset from a TEX/LATEX file prepared by the author.